Materials Research Express

PAPER

The resistance of an aluminide coating on a high-strength ASTM A29 steel subjected to a temperature of 850 °C

RECEIVED
7 March 2019

REVISED
28 April 2019

ACCEPTED FOR PUBLICATION
28 May 2019

PUBLISHED
5 June 2019

Mohammad Badaruddin[1], **Sugiyanto**[1] and **Dwi Asmi**[2]

[1] Department of Mechanical Engineering, Faculty of Engineering, Universitas Lampung, Bandar Lampung 35145, Indonesia
[2] Department of Physics, Faculty of Mathematics and Science, Universitas Lampung, Bandar Lampung 35145, Indonesia

E-mail: mbruddin@eng.unila.ac.id

Keywords: ASTM A29 steel, aluminide layer, high-temperature, oxidation resistance, alumina

Abstract

An ASTM A29 steel was coated with aluminide by dipping in a molten Al bath at 700 °C for 16 s. The resistance of ASTM A29 steel to high-temperature oxidation drastically decreased upon oxidation at 850 °C for 12 h, whereas the oxidation resistance of the aluminised steel subjected to hot dipping was higher (by 25-fold). The external part of the aluminide layer, which consists of Fe_2Al_5, $FeAl_2$, and FeAl (Cr, Si) phases scattered in the Fe_2Al_5 phase, was formed through the outward diffusion of Al and inward diffusion of Fe. The Fe_2Al_5 phase played an important role as a reservoir of Al atoms that form the alumina (Al_2O_3) scale, while Cr and Fe from the FeAl(Cr, Si) particles and accelerated the conversion of the metastable θ-Al_2O_3 phase to a stable α-Al_2O_3 phase. Consequently, the parabolic rate constants of aluminised steel decreased with extended oxidation time.

1. Introduction

A high strength ASTM A29 low alloy steel with a 1.10 Cr–0.25 Mo (wt%) can be a candidate material as replacement of high Cr–Mo steel grades and stainless-steel grades for high-temperature material applications in the petrochemical industry, power plants and transportations sectors. The ASTM A29 steel has good mechanical properties and is cheaper than those of high Cr–Mo steel grades and stainless-steel grades. However, the low Cr concentration in this steel is a critical issue, which limits its industrial application. Mazrouee and Raman [1] reported that the oxidation resistance of a 1.25 Cr–0.5 Mo steel exhibited a significant decrease in the temperature range of 500 °C–600 °C. At higher temperatures, the rapid oxidation kinetics for the chrome-moly steels with 0.5%–9% Cr and 0.5%–1% Mo were attributed to the loss of the protective Cr_2O_3 layer, which led to growing non-protective (Fe_2O_3), Fe_3O_4, and $(Fe, Cr)_3O_4$ scales. Therefore, the application of these steels is restricted above 600 °C [1–4].

To widen industrial applications in the temperature range of 700 °C–850 °C, the oxidation resistance of ASTM A29 steel needs to be improved by hot-dip aluminising (HDA) coating. HDA coating has been reported to be a simple, cost-effective method for improving the high-temperature resistance of steel and its alloys by forming a protective Al_2O_3 scale on the outer layer [5–7]. There are two types of HDA steel coating; (1) the aluminised Type 1 steel uses Al-(3%–10%)Si, and (2) the aluminised Type 2 steel uses relatively high purity Al. Adding a certain amount of Si into a molten Al bath reduces the thickness of the aluminide coating on the steel substrate [8, 9], which thins the aluminide coating, a pre-requisite to further manufacturing of aluminised steel components [10]. Therefore, an HDA coating with Al–Si is normally applied to low carbon steel, which is mainly used for automotive exhaust systems, furnace heat exchangers and other heat-resistant applications at 700 °C [5, 6]. However, the high-Si content in the intermetallic of FeAl layer growing on the low carbon steel substrate [5, 6] and on the high Cr–Mo steel substrate [7, 11] during oxidation in temperature range of 750 °C–850 °C had a detrimental effect, which led to the breakdown of protective Al_2O_3 layer due to local formation of iron oxide nodules. Therefore, the aluminised Type 2 steel has better oxidation resistance than that of the aluminised Type 1 steel [12]. Additionally, the aluminising Type 2 coating was applied to high strength AISI 4130 steel, which combines the strength of steel substrate and aluminide coating protections for superior hot-corrosion resistance

[13]. Because the thickness of the aluminide layer on the steel substrate determines the steel's mechanical properties [10], all industrial hot-dip aluminising type 2 processes allow the strict control of the coating reaction, by shortening the dipping time in few seconds.

Only a few publications on the high-temperature oxidation of aluminising Type 2 coating on high strength steel grades with the low Cr–Mo contents are available in the literature. Therefore, we experimentally investigated the resistance of aluminised Type 2 ASTM A29 steel on high-temperature oxidation in ambient air at 850 °C. A thermogravimetric analyser (TGA) was adopted to evaluate the oxidation kinetics of an ASTM A29 steel with and without aluminising coating. The microstructures, chemical composition and surface morphology of the aluminide layers after oxidation were examined.

2. Experimental procedure

A commercial ASTM A29 steel with chemical compositions of 0.3C-1.10Cr-0.25Mo-0.60Mn-0.035P-0.04S-0.30Si (wt%) was cut into specimens with 20 mm × 10 mm × 2 mm dimensions. A hole (1 mm diameter) was drilled into each specimen. The specimen surface was polished using 500–1000 emery paper and later ultrasonically cleaned using acetone and ethanol for a few seconds. Before coating, all specimens were ultrasonically neutralised using a 5% NaOH and a 10% H_3PO_4 solution for a few seconds. Next, the specimen surface was covered with an aluminium welding flux. The specimen was hung on a mini crane (Linear head (2FL10N-5 model) driven by a motor (2RK6RGN-CW2L model, with MSC controller) using a stainless-steel wire with 1 mm diameter. A motor automatically drove the mini crane at a constant speed of 14.3 mm min^{-1}, dipping the specimen into a molten Al–0.5Si (wt%) bath at 700 °C for 16 s. After the specimen was dipped, it was automatically pulled out from a molten Al bath and then cooled to room temperature. The oxide remaining on the specimen surface was then cleaned using a phosphoric acid/nitric acid/water solution (1:1:1 v/v) at room temperature.

To investigate the oxidation kinetics of the steels with and without the aluminium coating, specimens were subjected to air oxidation at 850 °C for 12 h using a TGA (Pyris 6 model). To evaluate the phase transformation and microstructures of the aluminide layer, aluminised steel specimens were oxidised in a box furnace at 850 °C for various times (1, 5 and 12 h) under static air. After the aluminised steel specimens were oxidised, they were removed from the furnace and then cooled to room temperature.

All aluminised steel specimens (before and after being oxidized) were characterized by means scanning electron microscopy (SEM; Jeol JSM 6390) with secondary electron imaging (SEI) for observing the microstructures and surface morphology of the aluminide layers. Additionally, Energy-dispersive spectroscopy (EDS) was also performed to analyse their chemical composition (expressed as atomic percentage, at%) for determining the phase formed in the aluminide layer.

3. Results and discussion

3.1. Characterisation of the aluminide coating

Figure 1(a) shows the typical microstructure of the aluminised ASTM A26 steel with the coating layer composing to two distinct regions; an aluminium layer (region I) and an intermetallic layer (region II). According to the Fe–Al phase diagram, the aluminide coating that was formed after the steel was dipped into a molten Al (~99 wt%) bath was dominated by an Al-rich layer and intermetallic compounds composed of $FeAl_3$ and Fe_2Al_5 phases [14]. EDS results in figure 1(a) verified that the chemical compositions of aluminide layer in regions I and II are consistent with Al layer (figure 1(b); Point (A), $FeAl_3$ layer (figure 1(c); Point (B), and Fe_2Al_5 layer (figure 1(d); Point (C). The aluminide coating consisted of an aluminium layer with low Fe, Si, and Cr concentrations (figure 1(b)). The solubilities of Si in the $FeAl_3$ and Fe_2Al_5 layers were approximately 1.4 at% and 2.44 at%, respectively. EDS results indicate that the solubilities of Cr were lower, 0.19 at% and 0.33 at%, respectively (figures 1(c) and 1(d)). According to the thermodynamic equilibrium, a Fe_2Al_5 phase with an orthorhombic structure and a high number of vacancies and defect paths initially formed along the *c* axis, ultimately contributing to the rapid growth of the Fe_2Al_5 phase [15].

The thicknesses of the aluminium and intermetallic layers were approximately 29 μm and 12 μm, respectively. According to Hwang *et al* [16], growth of an intermetallic layer and dissolution of marginal amounts of Fe into the molten aluminium occur simultaneously when steel is in contact with molten aluminium, and this growth is directly related to the loss of the steel substrate. The intermetallic layer had a homogeneous, dense structure. No pores and cracks could be observed in the aluminide coating. The interface between the aluminium topcoat and intermetallic layer was slightly uneven, and the intermetallic layer/steel substrate interface was relatively smooth because of its flat structure. This flat structure and the slow growth of

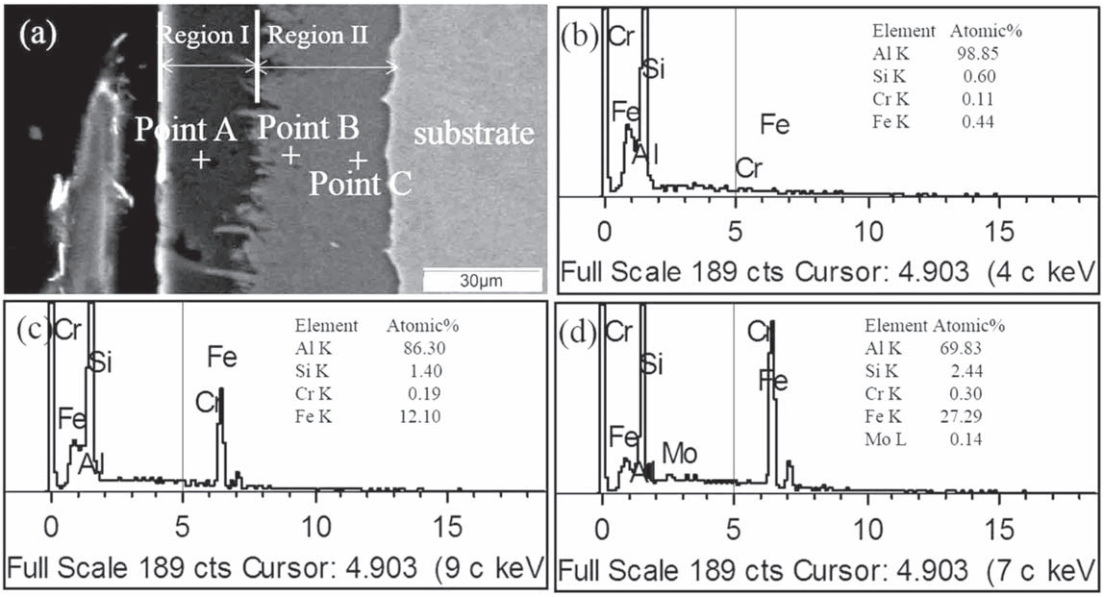

Figure 1. (a) SEI of the cross-sectional morphology of as coated steel and (b)–(d) EDS spectra of the aluminium and intermetallic layers.

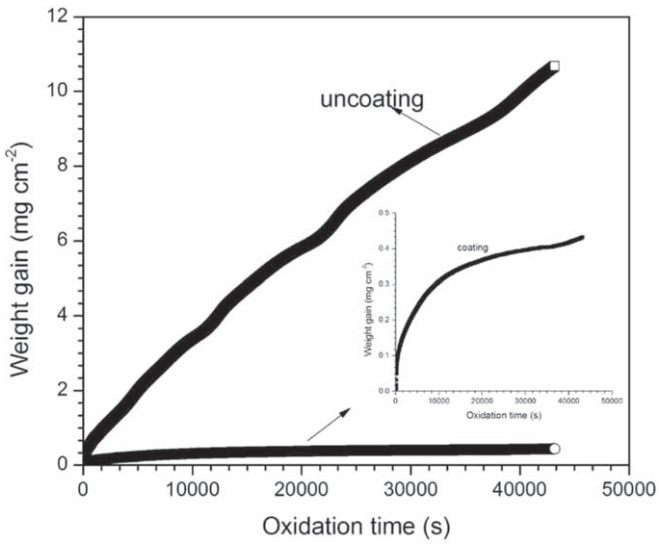

Figure 2. Oxidation kinetics curves for the ASTM A29 steel specimens with and without the aluminium coating.

the Fe_2Al_5 layer are due to the uniform pearlite microstructure and the high volume fraction of the cementite phase [16], respectively.

3.2. Resistance to high-temperature oxidation

Figure 2 shows plots of the weight gain of each specimen against the duration of oxidation indicate that the oxidation of the steel with and without aluminium coatings has parabolic kinetics. The weight gain of an ASTM A29 steel increased quickly. Hence, a 1.10 wt% Cr content of the steel is insufficient for forming a Cr_2O_3 layer that protects the steel during oxidation at 850 °C for 12 h.

That is, the oxidation kinetics rapidly increased. At the start of oxidation, the kinetics of the chemical reaction between iron and oxygen ions control the oxidation rate, resulting in rapid weight gain. Because of the low solubility of Cr in the oxide scale, Cr_2O_3 did not form, and consequently, the oxidation kinetics was rapid (figure 2). The Cr_2O_3 layer did not grow on the steel because of the depletion of Cr beneath the iron oxide layer to the lowest concentration [17]. Chromium was depleted toward the interface between the substrate and the iron-rich oxides Fe_3O_4 and FeO, by conversion to the $(Fe, Cr)_3O_4$ phase [4, 18].

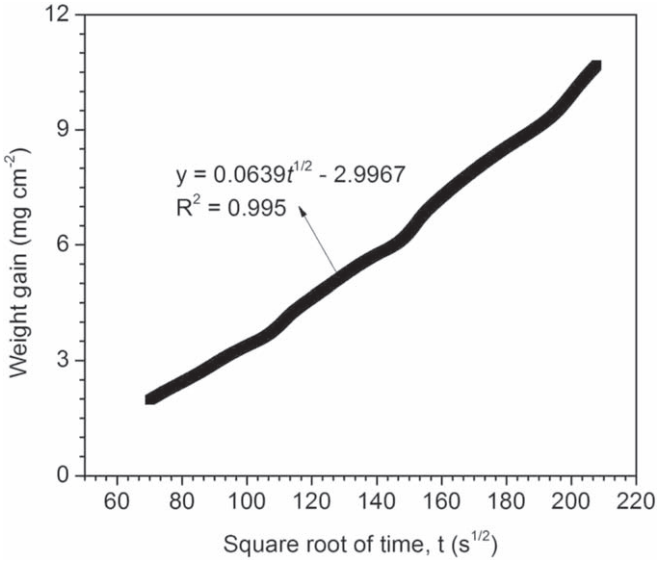

Figure 3. Plot of the weight gain versus the square root of time for an ASTM A29 steel in air oxidation at 850 °C for 12 h.

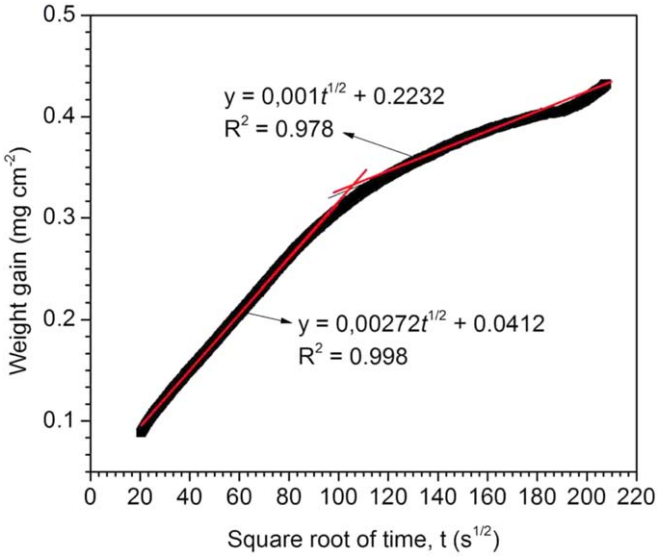

Figure 4. Plots of weight gain versus the square root of time for the aluminised ASTM A29 steel specimens after being oxidised at 850 °C for 12 h.

As can be observed in figure 2, the resistance of aluminised steel to high-temperature oxidation markedly increased. The aluminide layer protected the steel substrate against high-temperature oxidation by forming a protective aluminium oxide (Al_2O_3) layer. At 12 h of oxidation, the weight gain of steel with aluminium coating was approximately 0.432 mg cm^{-2}, which is 25-times less than that of the steel without the aluminium coating (10.675 mg cm^{-2}; figure 2).

Plots of the weight gain against exposure time for the uncoated and aluminised steel oxidised at 850 °C (figures 3 and 4, respectively) show parabolic behaviour. The parabolic rate constant (k_p) for uncoated steel calculated based on the oxidation at 1.4–12 h is approximately 4,083 $\times$ 10^{-6} g^2 cm^{-4} s^{-1}. As shown in figure 4, the oxidation rate constant ($k_p = 7.40 \times 10^{-12}$ g^2 cm^{-4} s^{-1}) was high during the first few hours of oxidation (0.12–2.78 h), subsequently decreasing to a steady-state value ($k_p = 1.00 \times 10^{-12}$ g^2 cm^{-4} s^{-1}) at 2.8–12 h. The k_p values in this study are an order of magnitude similar to those in previously reported studies [7, 19].

3.3. Characterization of aluminide layers

To elucidate the oxidation behaviour and the formation of intermetallic compounds in the aluminide layer, oxidation tests for aluminised steel specimens were performed. Figure 5(a) shows a cross-sectional image of the

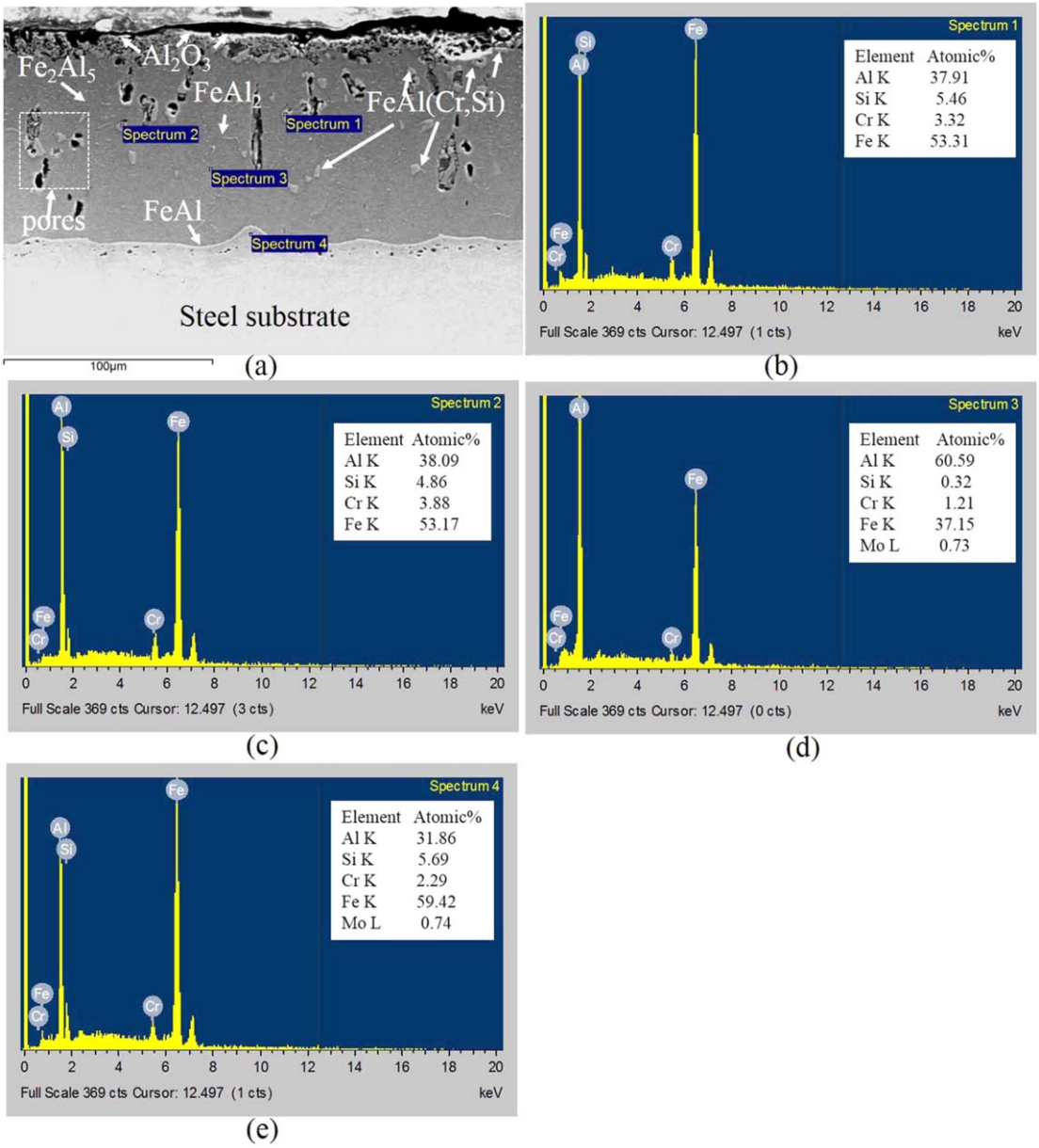

Figure 5. (a) Cross-sectional SEM image of the aluminide layer and (b)–(e) EDS spectra used in element analysis of the aluminide layer formed on the ASTM A29 steel after 1 h oxidation at 850 °C.

aluminised steel after oxidation for 1 h. The formation mechanism of the intermetallic compound was dominated by interdiffusion of Fe atoms in the substrate and Al atoms in the coating layer during high-temperature exposure. The aluminium and $FeAl_3$ layers of the as-coated specimen (figure 1(a)) transformed into Fe_2Al_5 and $FeAl_2$. Moreover, the high Si content and low Cr content of the Fe_2Al_5 layer rapidly decreased in the Fe-rich region because of diffusion coupling between the internal Al atoms and external Fe atoms, which generates regions of FeAl(Cr, Si) particles adjacent to the Fe_2Al_5 and $FeAl_2$ layers (figure 5(a)). Also, some voids that formed were dispersed in the outer aluminide layer (figure 5(a)). The intermetallic layer has a thickness of approximately 80 μm and consists of an Al_2O_3 thin layer on the surface adjacent to a thick $Fe_2Al_5/FeAl_2$ layer and a thin FeAl layer on the steel substrate. The inward diffusion of Al can dominate at this stage, and consumption by oxide growth is probably of minor importance in cavity formation. Also, pores also formed in the aluminide layer (figure 5(a)) because of phase transformation during high-temperature diffusion [20]. In contrast, the outward diffusion of Fe atoms from the steel substrate into the $Fe_2Al_5/FeAl_2$ layer resulted in the instability of the $Fe_2Al_5/FeAl_2$ layer and the formation of FeAl(Cr, Si) particles [7, 20] scattered in the $Fe_2Al_5/FeAl_2$ layer (figure 5(a)). EDS spectra (figures 5(b)–(d)) suggest that Si and Cr dissolved in the Fe_2Al_5, $FeAl_2$, and FeAl phases and that the Cr and Si content of the FeAl(Cr, Si) phase was substantially greater than that of the $FeAl_2$ phase (figures 5(b) and (c)). High concentrations of Cr and Si in the FeAl phase are due to the high

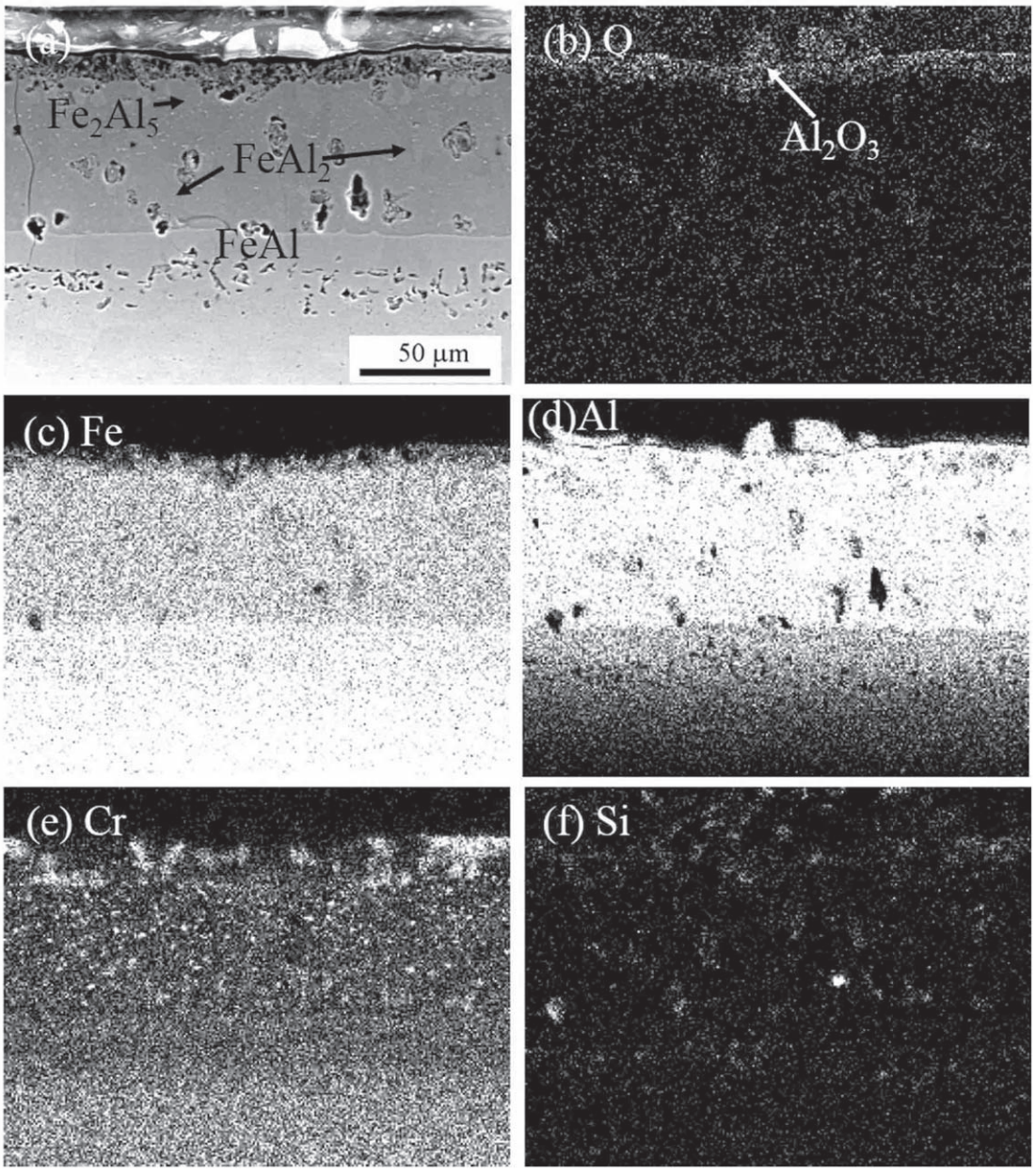

Figure 6. (a) SEM micrograph of the aluminide layer of the aluminised steel oxidised at 850 °C for 5 h, and (b)–(f) the corresponding EDS mapping results for O, Fe, Al, Cr, and Si.

solubility of both elements in the phase. EDS results for the $FeAl_2$ phase indicate that the solubility of Cr in the $FeAl_2$ phase is 0.49–1.2 at% and that the Fe_2Al_5 phase has a low Cr concentration (figure 1(c)).

SEM cross-sectional image of the aluminide layer of a specimen oxidised for up to 5 h (figure 6(a)) suggests that the Fe_2Al_5, $FeAl_2$, and FeAl phases rapidly grew on the steel substrate. Also, a thick Al_2O_3 layer formed (figure 6(b)). A continuous FeAl layer near the steel substrate gradually thickened via diffusion of Fe atoms into the $Fe_2Al_5/FeAl_2$ layer caused by the dilution of aluminium. This result is consistent with that obtained from the EDS x-ray map analysis (figures 6(c) and (d)). High Cr and Si concentrations in the FeAl(Cr, Si) phases, which became dispersed in the Fe_2Al_5 phase with increasing diffusion time, were still observed in the outer part of the aluminide layer.

This result is consistent with that obtained from x-ray map analysis (figures 6(e) and (f)). The solubilities of Cr and Si in both the FeAl(Cr, Si) particle region (2.29%–3.88%) and the continuous FeAl layer (4.86%–5.46%) were similar in atomic composition.

The k_p values of the aluminised steel at the initial stage were greater than those of the aluminised steel during steady-state oxidation (figure 4). This was because of the condensation of voids followed by the inward diffusion of oxygen through the voids and cracks, as well as the formation of metastable θ-Al_2O_3 [20] due to the outward diffusion of aluminium. After extended oxidation of aluminised steel (2.8–12 h), the k_p value of aluminised steel

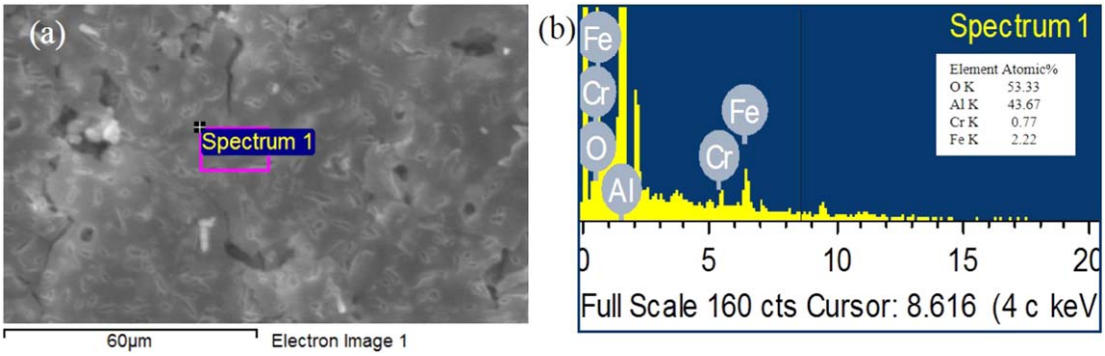

Figure 7. (a) SEM image of the surface morphology of the aluminised steel oxidised at 850 °C for 12 h, and (b) results of EDS spectral analysis of O, Al, Cr, and Fe.

(1.00×10^{-12} g^2 cm^{-4} s^{-1}) decreased seven-fold. Figure 7(a) shows the surface topography of aluminised steel exposed to 12 h of oxidation, as observed by SEI. With increasing oxidation time, the metastable alumina gradually transformed into the α-Al_2O_3 phase. Results of EDS element analysis (figure 7(b)) show that Fe and Cr atoms from the aluminide layer penetrated the α-Al_2O_3 scale because of the slightly high concentrations of Fe and Cr in the Al_2O_3 scale (figure 7(b)). Fe and Cr atoms detected in the alumina scale originated from the FeAl (Cr, Si) particles, and Si atoms were undetectable in the alumina scale (figure 7(b)). The Fe and Cr concentrations in the Al_2O_3 scale are similar to those reported by Lee *et al* [21]. The ability of both Fe and Cr to accelerate the transformation of θ-Al_2O_3 to α-Al_2O_3 [22–25] may be the main reason for the decrease in the rate of aluminised-steel oxidation in figure 4 due to the formation of the α-Al_2O_3 scale (figure 7(b)). Thus, a steady-state growth rate was observed over extended periods.

4. Conclusions

An ASTM A29 steel was subjected to hot-dip aluminium coating at 700 °C for an immersion time of 16 s in a molten Al-0.5% Si bath. The total thickness of the aluminide coating on the steel substrate was 41 μm. The Fe_2Al_5 layer on the steel substrate exhibited a planar structure, high homogeneity and a strong bond with the steel substrate. Upon coating by hot-dip aluminising process, the ASTM A29 steel resistance to high-temperature oxidation increased by a factor of 25. With increasing oxidation time, the oxidation rate constants of the aluminised steel decreased because of the formation of the protective α-Al_2O_3 scale. Growth of this scale was accelerated by the penetration of Fe and Cr ions into the θ-Al_2O_3 scale, which was predominantly caused by the high Fe concentration and low Cr concentration (<1%) in the alumina scale.

Acknowledgments

The authors would like to thank Kemenristekdikti for providing financial support through the Directorate of Research and Community Service (DRPM) for the National Strategy grant for financial support with contract No.: 009/SP2H/LT/DRPM/IV/2017.

ORCID iDs

Mohammad Badaruddin https://orcid.org/0000-0002-0427-2543

References

[1] Al-Mazrouee A and Raman R K S 2006 High temperature oxidation of Cr−Mo steels in the context of accelerated rupture testing for creep life prediction *J. Pressure Vessel Technol.* **129** 454–9
[2] Kumar R, Tewari V K and Prakash S 2016 Cyclic oxidation behaviour of 1Cr−0.5Mo (T11) boiler tube steel and its weldments in air at 900 °C *Oxid. Met.* **86** 89–98
[3] Abro M A and Lee D B 2017 Microstructural changes of Al hot-dipped P91 steel during high-temperature oxidation *Coatings* **7** 31
[4] Ehlers J, Young D J, Smaardijk E J, Tyagi A K, Penkalla H J, Singheiser L and Quadakkers W J 2006 Enhanced oxidation of the 9%Cr steel P91 in water vapour containing environments *Corros. Sci.* **48** 3428–54
[5] Wang C J and Chen S M 2006 The high-temperature oxidation behavior of hot-dipping Al–Si coating on low carbon steel *Surf. Coat. Technol.* **200** 6601–5

[6] Wang C J and Badaruddin M 2010 The dependence of high temperature resistance of aluminized steel exposed to water-vapour oxidation *Surf. Coat. Technol.* **205** 1200–5
[7] Chang Y Y, Tsaur C C and Rock J C 2006 Microstructure studies of an aluminide coating on 9Cr−1Mo steel during high temperature oxidation *Surf. Coat. Technol.* **200** 6588–93
[8] Yin F C, Zhao M X, Liu Y X, Han W and Li Z 2013 Effect of Si on growth kinetics of intermetallic compounds during reaction between solid iron and molten aluminum *Trans. Nonferrous Met. Soc. China* **23** 556–61
[9] Sree A S and Kumar E R 2014 Effect of heat treatment and silicon concentration on microstructure and formation of intermetallic phases on hot dip aluminized coating on Indian RAFMS *Fusion Sci. Technol.* **65** 282–91
[10] Zaba K 2012 Selected problems of formability of aluminised steel plates *Arch. Civ. Mech. Eng.* **12** 163–70
[11] Badaruddin M, Riza R T and Zulhanif 2018 The effect of diffusion treatment on the mechanical properties of hot-dip aluminum coating on AISI P20 steel *AIP Conf. Proc.* **1983** 050004
[12] Cheng W J and Wang C J 2013 High-temperature oxidation behavior of hot-dipped aluminide mild steel with various silicon contents *Appl. Surf. Sci.* **274** 258–65
[13] Badaruddin M, Wang C J, Saputra Y and Rivai A K 2015 High temperature corrosion of aluminized AISI 4130 steel with the different composition of $NaCl/Na_2SO_4$ deposits *Makara J. Technol.* **19** 45–6
[14] Kattner U R and Burton B P 1992 *Alloy Phase Diagrams* 3 (United States of America: ASM International)
[15] Cheng W J and Wang C J 2009 Growth of intermetallic layer in the aluminide mild steel during hot-dipping *Surf. Coat. Technol.* **204** 824–8
[16] Hwang S H, Song J H and Kim Y S 2005 Effects of carbon content of carbon steel on its dissolution into a molten aluminum alloy *Mater. Sci. Eng.* A **390** 437–43
[17] Raman R K S 2000 Relevance of high-temperature oxidation in life assessment and microstructural degradation of Cr–Mo steel weldments *Metall. Mat. Trans.* A **30** 3101–8
[18] Chaliampalias D, Vourlias G, Pavlidou E and Chrissafis K 2013 High temperature oxidation of Cr–Mo–V tool steel in carbon dioxide *J. Therm. Anal. Calorim.* **113** 1309–15
[19] Chang Y Y, Cheng W J and Wang C J 2009 Growth and surface morphology of hot-dip Al–Si on 9 Cr–1 Mo steel *Mater. Charac.* **60** 144–9
[20] Cheng W J and Wang C J 2013 Effect of chromium on the formation of intermetallic phases in hot-dipped aluminide Cr–Mo steels *Appl. Surf. Sci.* **277** 139–45
[21] Lee D B, Kim G Y and Kim J G 2003 The oxidation of Fe_3Al−(0, 2, 4, 6%)Cr alloys at 1000 °C *Mater. Sci. Eng.* A **339** 109–14
[22] Hayashi S, Takada Y, Yoneda S and Ukai S 2016 Metastable-Stable phase transformation behavior of Al_2O_3 scale formed on Fe–Ni–Al Alloys *Oxid. Met.* **86** 151–64
[23] Zhan Q, Zhao W, Yang H, Hatano Y, Yuan X, Nozaki T and Zhu X 2015 Formation of α-alumina scales in the Fe–Al(Cr) diffusion coating on China low activation martensitic steel *J. Nucl. Maters.* **464** 135–9
[24] Huang Y and Peng X 2016 The promoted formation of α-Al_2O_3 scale on a nickel aluminide with surface Cr_2O_3 particles *Corros. Sci.* **112** 226–32
[25] Shaaban A, Hayashi S and Azumi K 2015 Promotion of α-Al_2O_3 formation on an Ni–Al alloy using a Ni–Fe_2O_3 nano-composite seeding layer *Surf. Coat. Technol.* **266** 113–21